Acta Crystallographica Section D
Biological Crystallography
ISSN 0907-4449

Structure of human erythrocyte catalase

Tzu-Ping Ko,[a]* Martin K. Safo,[b] Faik N. Musayev,[b] Martino L. Di Salvo,[b] Changqing Wang,[b] Shih-Hsiung Wu[a] and Donald J. Abraham[b]

[a]Institute of Biological Chemistry, Academia Sinica, Taipei 11529, Taiwan, and [b]Institute for Structural Biology and Drug Discovery, Virginia Commonwealth University, Richmond, VA 23219, USA

Correspondence e-mail: kotping@gate.sinica.edu.tw

Received 28 July 1999
Accepted 7 December 1999

PDB Reference: human erythrocyte catalase, 1qqw.

Catalase (E.C. 1.11.1.6) was purified from human erythrocytes and crystallized in three different forms: orthorhombic, hexagonal and tetragonal. The structure of the orthorhombic crystal form of human erythrocyte catalase (HEC), with space group $P2_12_12_1$ and unit-cell parameters a = 84.9, b = 141.7, c = 232.5 Å, was determined and refined with 2.75 Å resolution data. Non-crystallographic symmetry restraints were employed and the resulting R value and R_{free} were 0.206 and 0.272, respectively. The overall structure and arrangement of HEC molecules in the orthorhombic unit cell were very similar to those of bovine liver catalase (BLC). However, no NADPH was observed in the HEC crystal and a water was bound to the active-site residue His75. Conserved lattice interactions suggested a common growth mechanism for the orthorhombic crystals of HEC and BLC.

1. Introduction

The presence of reactive oxygen species (ROS) in all aerobic organisms is harmful to DNA and other cellular components and causes disease and ageing if not immediately scavenged (Halliwell & Gutteridge, 1990). Hydrogen peroxide (H_2O_2) is one of the ROS that decomposes into free hydroxyl radicals, the most deleterious species of activated oxygen (Scandalios, 1997). Catalase (E.C. 1.11.1.6) catalyzes the reaction

$$2H_2O_2 \rightarrow 2H_2O + O_2$$

and is directly involved in eliminating oxidative stress. Loss of the catalase gene decreased the viability of fruit flies (Griswold *et al.*, 1993) and reduced catalatic activity in *Xeroderma pigmentosum* cells could be directly related to impaired DNA repair (Quilliet *et al.*, 1997), while stable overexpression of the catalase gene markedly attenuated the H_2O_2-induced toxic effect in immortalized neural cells (Mann *et al.*, 1997). Catalase was shown to be effective in inhibiting the degeneration of neurons (Busciglio & Yankner, 1995). A growth-promoting factor derived from human erythrocytes with a wide target-cell spectrum was also identified as catalase (Takeuchi *et al.*, 1995).

Human erythrocyte catalase (HEC) is a tetrameric protein of 244 kDa, comprising four identical subunits of 59.7 kDa plus four heme groups and four NADPH molecules (Bonaventura *et al.*, 1972; Kirkman & Gaetani, 1984). It is very similar to bovine liver catalase (BLC), which is the only known mammalian catalase that has had its three-dimensional structure determined (Murthy *et al.*, 1981). The human gene of catalase has been cloned (Quan *et al.*, 1986). Besides the 25-residue extension at the C-terminus, HEC differs from BLC in 43 amino-acid residues. In BLC, the four subunits are related by a 222 point-group molecular symmetry. Catalases from other sources, *e.g.* the *Proteus mirabilis* catalase (PMC; Gouet *et al.*, 1995), catalase-A from *Saccharomyces cerevisiae* (SCC-A; Maté, Zamocky *et al.*, 1999) and a larger catalase from *Escherichia coli* (HPII; Bravo *et al.*, 1995), have a similar core structure and the same tetrameric organization as BLC. The tetrameric enzyme contains a central cavity and several channels that reach the active-site heme groups and facilitate the entry and exit of substrates and products (Fita & Rossmann, 1985; Gouet *et al.*, 1996; Sevinc *et al.*, 1999).

Because of their large molecular size, catalases have been exploited in a number of crystal-growth experiments (Sato *et al.*, 1993; Malkin *et al.*, 1995). HEC was observed as two-dimensional crystals by electron microscopy (Harris *et al.*, 1993; Harris & Holzenburg, 1995), but three-dimensional crystals have not been reported until recently (Maté, Lombardia *et al.*, 1999). In this paper, we describe the purification of HEC and its crystallization in new crystal forms. We have also determined the structure of HEC in an orthorhombic crystal by molecular replacement. This turned out to be very similar to the orthorhombic BLC crystals recently reported by Ko *et al.* (1999). Packing and intermolecular interactions explained the growth mechanism of the BLC crystals, which may also apply to the HEC crystals.

Table 1
Data-collection and structure-refinement statistics.

Numbers in parentheses are for the highest resolution shells.

Data collection	
Unit-cell parameters (Å)	a = 84.9, b = 141.7, c = 232.5
Resolution (Å)	233–2.73 (2.82–2.73)
Number of observations	131236 (7325)
Unique reflections	64674 (4606)
Completeness (%)	86.0 (67.0)
$R_{\rm merge}$ (%)	10.9 (35.4)
Crystallographic refinement	
Resolution range (Å)	40–2.75 (2.85–2.75)
Number of reflections (all data)	59969 (4498)
With $F > 2\sigma_F$ cutoff	44450 (2417)
R value based on 92% data	23.9 (34.6)
With $F > 2\sigma_F$ cutoff	20.6 (29.9)
$R_{\rm free}$ for 8% test data set	31.6 (43.2)
With $F > 2\sigma_F$ cutoff	27.2 (39.5)
R.m.s.d. from ideal bond length (Å)	0.005
R.m.s.d. from ideal bond angle (°)	0.897
Dihedral angles	
In most favored regions (%)	80.3
In additional allowed regions (%)	18.9
Average B values (Å^2)	
16622 non-H atoms	12.79
7988 backbone atoms (N, C$^\alpha$, C, O)	12.59
8069 side-chain atoms (others)	12.69
172 heme atoms	13.43
393 solvent atoms	18.69

2. Materials and methods

2.1. Purification, crystallization and data collection

DEAE–Sephadex A-50, CM–Sephadex C-50, 2-mercaptoethanol and PMSF were purchased from Sigma (St Louis, Missouri, USA). All other chemicals were from Fisher Scientific (Springfield, New Jersey, USA). The procedure was a modification of Morikofer-Zwez *et al.* (1969). Outdated packed red blood cells were obtained from the Virginia Blood Bank. About 600 ml of red blood cells were mixed with two volumes of buffer containing 10 m*M* 2-mercaptoethanol, 10 m*M* EDTA, 10 m*M* 4-aminocaproic acid, 1 m*M* PMSF, 10 m*M* potassium phosphate pH 7.0 plus 10%(*v*/*v*) cold toluene. After homogenization and centrifugation to remove the upper fat layer, ammonium sulfate was added to the suspension to 50% saturation. The pellet was washed with 500 ml of buffer containing ammonium sulfate at 45% saturation, resuspended in a minimum volume of buffer at pH 7.2 and dialyzed against the same buffer. This sample was then loaded onto a DEAE–Sephadex A-50 column equilibrated with the pH 7.2 buffer. A green-brown band was observed to bind to the top of the column. After extensive washing with the buffer, the band was eluted using a 0–250 m*M* NaCl gradient. Fractions having an A_{406}/A_{278} ratio higher than 0.65 were pooled and the protein was precipitated by adding ammonium sulfate to 50% saturation. The pellet was dialyzed against a buffer containing 5 m*M* 2-mercaptoethanol, 0.2 m*M* EDTA, 10 m*M* potassium phosphate pH 6.5 and loaded onto a CM–Sephadex C-50 column equilibrated with the same buffer. The flow-through solution (part *A*) which had an A_{406}/A_{278} of 1.04 was found to contain the purest catalase, while most of the proteins were bound to the column, and fractions containing catalase (part *B*) were eluted with a 0–250 m*M* potassium phosphate gradient. The total yield was 110 mg, comprising 45 mg in part *A* and 65 mg in part *B*. To grow crystals, part *A* was used after concentration by ammonium sulfate precipitation and dialysis against 50 m*M* KCl, 1 m*M* 2-mercaptoethanol, 0.2 m*M* EDTA, 20 m*M* sodium acetate pH 5.2.

Crystallization conditions were screened using the hanging-drop vapor-diffusion technique (McPherson, 1982). Drops were set up by mixing equal volumes of the dialyzed catalase solution, which contained 16 mg ml^{-1} protein, and the reservoir. Various precipitants including low and high molecular weight polyethylene glycol (PEG), 3-methyl-2,4-pentanediol, ammonium sulfate, potassium sodium tartrate and sodium chloride were tested over the pH range 6.0–9.0. After about a week at room temperature, crystals grew in droplets of the screen with PEG as the precipitant; two crystal forms were obtained after optimization. The green-brown colored rod-like orthorhombic crystals were first observed in drops comprising 5 µl protein solution and 5 µl reservoir solution consisting of 6–7% PEG 20 000 and 0.1 *M* MES pH 6.2. Further improvement to the size of the crystals and the reproducibility was achieved by raising the pH value to 6.7 and lowering the protein concentration to about 8 mg ml^{-1}. These crystals reached maximum dimensions of 0.8 × 0.4 × 0.3 mm in about two weeks. They diffracted X-rays to 2.6 Å resolution and belong to space group $P2_12_12_1$, with unit-cell parameters a = 84.9, b = 141.7, c = 232.5 Å. Diffraction intensities were measured at room temperature to 2.73 Å using an R-AXIS II imaging-plate detector system and a rotating-anode generator (Rigaku RU-200) operating at 50 kV and 180 mA. Data were processed using the *BIOTEX* software (Molecular Structure Corporation, The Woodlands, Texas, USA) and the *CCP*4 suite (Collaborative Computational Project, Number 4, 1994). Statistics are listed in Table 1.

The second crystal form, having approximately hexagonal bipyramidal morphology, grew in drops equilibrated against a reservoir containing 5.5% PEG 8000, 15 m*M* $MgSO_4$, 70 m*M* Tris buffer at the high pH value of 8.5. The crystals were of red–brown color and reached maximum dimensions of 0.4 × 0.3 × 0.2 mm. This crystal form belongs to a hexagonal space group but diffracted poorly; no attempt was made to determine the space group. The unit-cell parameters are $a = b$ = 88.3, c = 257.1 Å, similar to the unit-cell dimensions reported by Maté, Lombardia *et al.* (1999) in their characterization of the HEC crystal. Their crystal belonged to the hexagonal space group $P6_422$; it is most likely that our crystal also belongs to this space group. A further search for crystallization conditions yielded a third crystal form. The reservoir contained 0.7 *M* potassium sodium tartrate and 0.1 *M* HEPES buffer pH 7.0. Protein concentration before mixing was 16 mg ml^{-1} and the initial drop volume was 3 µl. These crystals grew slowly over 4–6 months at room temperature and had well defined morphology. The final crystals had dimensions of 0.32 × 0.25 × 0.25 mm and diffracted X-rays to about 2.9 Å resolution. The crystals belonged to the space group $I4_1$, with unit-cell parameters $a = b$ = 202.9, c = 152.4 Å.

2.2. Structure determination and refinement

The structure determination was carried out using the orthorhombic crystal of HEC and the BLC model (PDB entry 4blc; Ko *et al.*, 1999). Because the space group and unit-cell dimensions of the BLC and HEC crystals were almost identical, the molecular packing and overall protein fold were presumed to be identical. Therefore, no rotational or translational search with the model was necessary. Direct application of the BLC model to the HEC crystal yielded a correlation coefficient of 0.74 and an R value of 0.30, calculated by the program *AMoRe* (Navaza, 1994) using data in the resolution range 8.0–4.0 Å. Subsequent refinement of the model employed the program *X-PLOR* (Brünger, 1992*a*). Model building was carried out on an SGI Octane using the

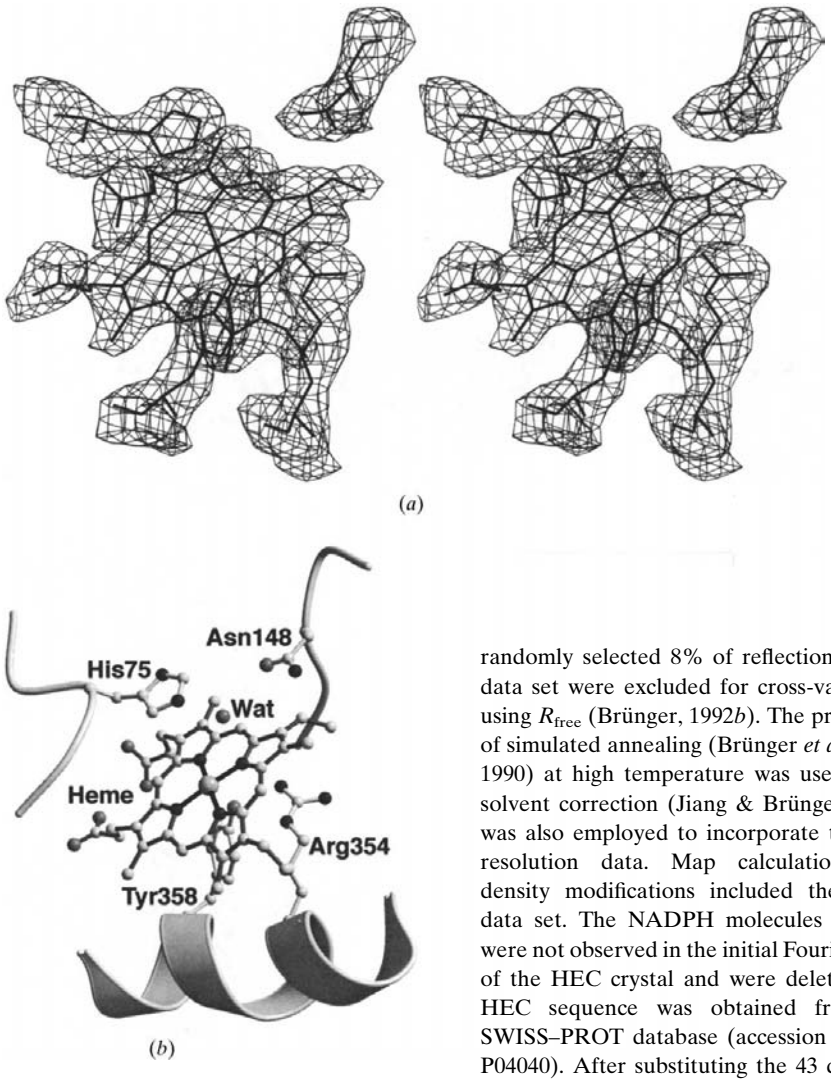

Figure 1
Stereodiagram and ribbon drawing of the heme group in HEC (subunit *A*). The residues Arg354 and Tyr358 on the proximal side and His75 and Asn148 on the distal side as well as the substrate water are shown. The electron-density map was calculated using DM phase angles and contoured at the 1.5σ level. The programs *TOM, MOLSCRIPT* and *Raster3D* were used in making this figure.

program *O* (Jones *et al.*, 1990). The *CCP*4 suite (Collaborative Computational Project, Number 4, 1994) was used for density modification. The stereochemistry of the model was evaluated by *PROCHECK* (Laskowski *et al.*, 1993). The programs *TOM* (Jones, 1982), *MOLSCRIPT* (Kraulis, 1991), *Raster3D* (Merritt & Murphy, 1994) and *GRASP* (Nicholls *et al.*, 1991) were used to produce the figures.

Rigid-body refinement using the orthorhombic BLC model with all solvent molecules removed gave an initial R value of 0.38 for all data. In the following refinement, a randomly selected 8% of reflections in the data set were excluded for cross-validation using $R_{\rm free}$ (Brünger, 1992*b*). The procedure of simulated annealing (Brünger *et al.*, 1987, 1990) at high temperature was used; bulk-solvent correction (Jiang & Brünger, 1994) was also employed to incorporate the low-resolution data. Map calculations and density modifications included the entire data set. The NADPH molecules in BLC were not observed in the initial Fourier maps of the HEC crystal and were deleted. The HEC sequence was obtained from the SWISS–PROT database (accession number P04040). After substituting the 43 different amino-acid residues in BLC with those of HEC, preliminary refinement of the model gave an R value and an $R_{\rm free}$ of 0.30 and 0.37, respectively. This provided starting phase angles for subsequent density modification (DM) with solvent flattening, histogram matching and fourfold molecular averaging using the *CCP*4 suite (Collaborative Computational Project, Number 4, 1994). In DM, $R_{\rm free}$ improved from 0.362 to 0.304 and correlation coefficients between the subunit densities improved from 0.783–0.795 to 0.919–0.925. The map calculated using DM phases showed well defined density for the entire tetramer and additional densities for water molecules. Fig. 1 shows a DM map around one of the heme groups. However, in the N- and C-terminal regions the densities were still insufficient to allow tracing of the missing residues 1–3 and 503–527. The refinement proceeded with non-crystallographic symmetry (NCS) restraints. No improvement in the terminal regions was seen in the maps recalculated after refinement.

3. Results and discussion

3.1. Crystallographic refinement and structural comparison

The final model contained 1997 amino-acid residues in four subunits (named *A, B, C* and *D*), four heme groups and 393 waters. The polypeptide chain of each subunit had residues 4–502. An additional residue, Glu503, was included as an alanine in subunit *B* because its backbone was visible in the electron-density maps. With strong NCS and stereochemical restraints applied, the R value and $R_{\rm free}$ were 0.239 and 0.316, respectively, for all data in the resolution range 40–2.75 Å. For data with a $2\sigma_F$ cutoff, the corresponding values became 0.206 and 0.272, respectively. The average coordinate errors were between 0.30 and 0.35 Å, as estimated by a Luzzati plot (Luzzati, 1952). Other statistical values are listed in Table 1. The Ramachandran plot from *PROCHECK* showed that 80.3% of non-glycine and non-proline residues were in the most favored regions and only one residue, Ser217, in all four subunits was in a disallowed region. It had φ and ψ angles of 73 ± 5 and $-59 \pm 4^\circ$, respectively. Similar conformations were observed in the corresponding residues of other catalase models, *e.g.* Ser216 in BLC and Ile274 in HPII. The average temperature factor of 12.8 Å^2 was lower than the value of about 20 Å^2 estimated by a Wilson plot (Wilson, 1950). This was probably a consequence of the low resolution of the data set.

The overall protein fold of HEC is identical to BLC, with a core structure of an eight-stranded β-barrel surrounded by a number of α-helices (Fita & Rossmann, 1985). The four subunits were organized about three perpendicularly intersecting dyad axes and express 222 point-group symmetry. The r.m.s.d. coordinate differences between the four subunits were 0.156 Å for the backbone atoms, 0.400 Å for the side chains and 0.125 Å for the heme groups, reflecting appropriate maintenance of the NCS restraints. The entire HEC and BLC tetramers could also be superimposed with an r.m.s.d. of 0.387 Å for 1996 equivalent C^α atoms. The r.m.s.d. for the 7984 backbone atoms was 0.423 Å and was 1.006 Å for the 7740 equivalent atoms in the side chains. The four heme groups deviated by an r.m.s.d. of 0.724 Å or 0.41–0.53 Å when superimposed separately. Fig. 2 shows the two catalase models superposed. The 43 different amino-acid residues appear to be randomly distributed throughout the protein. Nevertheless, the β9 strand, which is involved in an association with its symmetry-

related equivalent, contains six amino-acid substitutions. The ligand to the heme iron, Tyr358 of HEC, as well as the essential His75 assumed virtually identical conformations to those observed in BLC. Other active-site residues, more than 30 in number, which constitute the binding pocket and proximal and distal sides of the heme group, are all conserved in HEC and BLC, except for the substitution of Ala157 in BLC by Pro158 in HEC. This residue is in contact with the vinyl group of the heme pyrrole ring I and has α-helical conformation. It is the first residue of the α3 helix and is well accommodated.

At 2.75 Å resolution, not much information could be extracted from the HEC model, even though it was refined with strong stereochemical and fourfold NCS restraints. The major difference between the two almost isomorphous orthorhombic crystal structures of HEC and BLC was the absence of bound NADPH molecules in HEC. The 19 amino-acid residues of BLC involved in contact with NADPH are also conserved in HEC, with the exception of Asp212 in BLC *versus* Asn213 in HEC. The acidic side chain of Asp212 in BLC forms hydrogen bonds with the 3′-phosphate of the NADPH molecule. Substitution by Asn213 in HEC neutralizes the side chain yet still maintains hydrogen-bonding capacity. Comparison with the BLC structure showed that the guanidinium group of Arg203 in HEC was rotated 60° away from the NADPH-binding position to form hydrogen bonds with the phenolic O atom of Tyr215. The 76 backbone atoms of the 19 residues that line the NADPH pocket in HEC and BLC could be superimposed with r.m.s.d.s in the range 0.30–0.46 Å, depending on the subunits compared. The side chains deviated by an r.m.s.d. of 0.72–0.86 Å for 99 equivalent atoms. Because the differences are small, all of these residues in HEC can be readily adjusted to make proper interactions with the NADPH molecule as in BLC. Therefore, the binding site should be intact and functional. In addition, the side-chain amino group of Lys306 in HEC was close to the pyrophosphate group of NADPH in BLC, with distances of 1.7–2.4 Å. By forming salt bridge and/or hydrogen bonds with the pyrophosphate, this lysine should further strengthen the binding of NADPH to HEC. The corresponding residue in BLC is Gly305 and similar arrangement is not possible. In the orthorhombic BLC structure, the side chain of Phe197 had two conformations '*A*' and '*B*', which differ by a χ_1 rotation of 120°; in the trigonal BLC crystal (PDB entry 7cat), it had the '*B*' conformation; in the current HEC model, all equivalent Phe198 had the '*A*' conformation. In either conformation, this side chain makes close contacts with the nicotinamide and adenine groups of the NADPH molecule; it is uncertain which conformation would be favored in binding NADPH.

In the structure of SCC-A, the NADP(H) site had only a partial occupancy of about 50% (Maté, Zamocky *et al.*, 1999). The NADPH molecules in the orthorhombic BLC crystals had extremely high temperature factors (Ko *et al.*, 1999). The results suggested weak binding of the dinucleotide in these crystals. Kirkman & Gaetani (1984) showed that both HEC and BLC bind strongly to NADPH but not to $NADP^+$, with affinities NADPH > NADH >> $NADP^+$ > NAD^+. In the present study, the enzyme was purified from blood after prolonged storage and no NADPH was added. Most of the coenzyme would have been oxidized and readily dissociated from the HEC molecules. Nevertheless, the specific catalytic activity of the purified protein solution or redissolved HEC crystals was comparable with that of BLC (data not shown). This is consistent with the results of PMC, which can be fully active with NADPH removed (Gouet *et al.*, 1995).

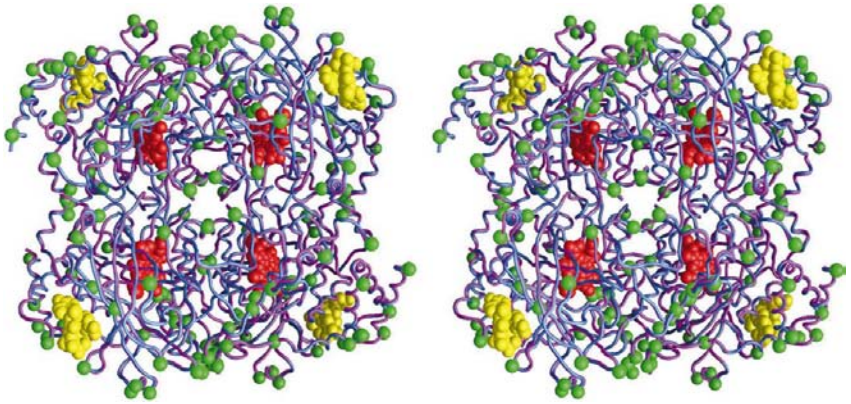

Figure 2
Superposition of the HEC (colored blue) and BLC (colored purple) models. The C^α atoms of the variable residues are shown in green. Heme groups are shown in red. The NADPH molecules which were observed in BLC but not in HEC are shown in yellow. The figure was drawn using *GRASP*.

3.2. Solvent model and lattice contacts

The orthorhombic HEC crystal had a specific volume (Matthews, 1968) of V_m = 2.87 $Å^3\,Da^{-1}$, corresponding to a solvent content of 57%. There were 384 bound waters in the BLC crystal structure and 393 in the current HEC model. When the two models were superimposed, 38 pairs of equivalent waters were matched within 1.5 Å distance. If the matching criterion was 1.0 Å, the number of equivalents would be 19. These are few compared with the 99 equivalent waters in the trigonal and orthorhombic crystal structures of BLC (Fita *et al.*, 1986; Ko *et al.*, 1999). The 19 conserved waters showed a featureless pattern of distribution, except those bound to the O1A atoms of heme propionate and Thr361 OG1 atoms in all four subunits. In addition, a notable active-site water bound to the NE2 of His75 (at a distance of 2.59–2.85 Å) and possibly OD1 of Asn148 (at a distance of 3.21–3.89 Å) was also observed in each subunit. These 'substrate' waters had low temperature factors and strong electron densities in the Fourier maps (Fig. 1). The equivalent solvent molecules have been observed in a number of other catalases, including an azide ion in SCC-A (Maté, Zamocky *et al.*, 1999) and a water in HPII (Bravo *et al.*, 1995), but not in either crystal form of BLC. On the proximal side of the heme group, solvent channels with 3–4 bound water molecules were visible, but they appeared not to be directly involved in interaction with the active site. The channels were connected to the central cavity of the HEC tetramer, in which there were 16 waters.

Because the HEC crystal is almost identical or quasi-isomorphous to the BLC crystal, the interactions between the tetrameric catalase molecules should be very similar. This was verified by analyzing the crystal contacts. Like BLC, an HEC molecule was in contact with four symmetry-related neighbors in the crystal and the interactions could be divided into two types. The first type (interface I) is between molecules related by the 2_1 screw axis

Table 2
Possible residues involved in crystal contacts.

Interface I: molecules related by (i) x, y, z and (ii) $-x, \frac{1}{2}+y, \frac{1}{2}-z$.

Residue 1	Atom	Residue 2	Atom	d (Å)	Comments
Gln*A*424	NE2	Ser*C*276	OG	3.44	Hydrogen bond (salt bridge),
Glu*A*290	OE1	Lys*C*243	NZ	> 4	could be mediated by water
Glu*B*290	OE1	Lys*C*106	NZ	> 4	(salt bridge),
				< 3	By side-chain rotations
Glu*B*428	OE2	Lys*C*315	NZ	3.14	Salt bridge
Phe*B*432	CE1	Thr*C*88	CB	3.84	vdW contact
Pro*C*46	CB	Ile*C*103	CG2	3.98	vdW contact
Arg*C*47	NH1	Gly*C*104	O	2.8	Hydrogen bond

Interface II: molecules related by (i) x, y, z and (ii) $-\frac{1}{2}+x, \frac{1}{2}-y, 1-z$.

Residue 1	Atom	Residue 2	Atom	d (Å)	Comments
Asn*A*449	O	Glu*D*453	N	3.01	Hydrogen bond
Asn*A*449	O	Arg*D*456	NH2	3.26	Hydrogen bond
Asn*A*452	ND2	Gln*D*455	OE1	3.28	Hydrogen bond
Glu*A*453	N	Asn*D*449	O	3.19	Hydrogen bond
Gln*A*455	OE1	Asn*D*452	ND2	3.46	Hydrogen bond
Arg*A*456	NH2	Asn*D*449	O	2.68	Hydrogen bond

parallel to the *b* axis. It covered a surface area of 563 Å^2 on one molecule and 541 Å^2 on the other. There were at least 14 water molecules involved, which contributed an additional 380 Å^2 to the interface area. The second type (interface II) is between molecules related by the screw axis parallel to the *a* axis and, by coincidence, a non-crystallographic pseudo-dyad axis. The contact areas were 304 Å^2 and 287 Å^2 on the two protein molecules and 141 Å^2 on six waters. Interface I covered twice as much surface area as did interface II. Specific interactions could not be identified for sure owing to the low resolution and the NCS restraints of the refinement. Nevertheless, a few possible contacts are listed in Table 2. The salt bridges of Glu*B*290–Lys*C*106*[1] and Glu*B*428–Lys*C*315* in HEC correspond to Glu*B*289–Arg*C*105* and Asp*B*427–Lys*C*314* in BLC. In addition to the polar residues, interface I contains a hydrophobic patch of Phe*B*432, Pro*C*46, Thr*C*88* and Ile*C*103*. Identical non-polar interactions were also observed for BLC. Interface II contains no salt bridge but involves several backbone atoms. In this region, the C-terminus of the α10 helix of subunit *A* was directed to the N-terminus of the α11 helix of subunit *D** and *vice versa*. Thus, the two antiparallel helices were symmetrically extended across the interface to the other molecule by dipole–dipole interactions and hydrogen bonding. Consequently, in the HEC crystal both regions of lattice contacts were largely conserved with respect to the BLC crystal, although NADPH was not observed in HEC and waters were not involved in BLC. The non-conserved contacts were a consequence of non-conserved residues in these regions, which made a different set of hydrogen-bonding interactions between side chains. Presumably, HEC and BLC share the same crystal-growth mechanism in the orthorhombic space group as described by Ko *et al.* (1999), *i.e.* by formation of half unit-cell layers. Within a layer, molecules are associated through the stronger interface I; between adjacent layers, they interact through the weaker interface II.

[1] The asterisks designate residues in symmetry-related molecules.

We thank Professor Donatella Barra and Dr Bruno Maras for protein sequencing. This work was supported by the National Institutes of Health (Grant HL-32793).

References

Bonaventura, J., Schroeder, W. A. & Fang, S. (1972). *Arch. Biochem. Biophys.* **150**, 606–617.

Bravo, J., Verdaguer, N., Tormo, J., Betzel, C., Switala, J., Loewen, P. C. & Fita, I. (1995). *Structure*, **3**, 491–502.

Brünger, A. T. (1992*a*). *X-PLOR Version* 3.1. *A System for X-ray Crystallography and NMR.* Yale University Press, New Haven, Connecticut, USA.

Brünger, A. T. (1992*b*). *Nature (London)*, **355**, 472–474.

Brünger, A. T., Krukowski, A. & Erickson, J. (1990). *Acta Cryst.* A**46**, 585–593.

Brünger, A. T., Kuriyan, J. & Karplus, M. (1987). *Science*, **235**, 458–460.

Busciglio, J. & Yankner, B. A. (1995). *Nature (London)*, **378**, 776–779.

Collaborative Computational Project, Number 4 (1994). *Acta Cryst.* D**50**, 760–763.

Fita, I. & Rossmann, M. G. (1985). *J. Mol. Biol.* **185**, 21–37.

Fita, I., Silve, A. M., Murthy, M. R. N. & Rossmann, M. G. (1986). *Acta Cryst.* B**42**, 497–515.

Gouet, P., Jouve, H. M. & Dideberg, O. (1995). *J. Mol. Biol.* **249**, 933–954.

Gouet, P., Jouve, H. M., Williams, P. A., Andersson, I., Andreoletti, P., Nussaume, L. & Hajdu, J. (1996). *Nature Struct. Biol.* **3**, 951–956.

Griswold, C. M., Matthews, A. L., Bewley, K. E. & Mahaffey, J. W. (1993). *Genetics*, **134**, 781–788.

Halliwell, B. & Gutteridge, J. M. C. (1990). *Methods Enzymol.* **186**, 1–85.

Harris, J. R., Engelharde, H., Volker, S. & Holzenburg, A. (1993). *J. Struct. Biol.* **111**, 22–33.

Harris, J. R. & Holzenburg, A. (1995). *J. Struct. Biol.* **115**, 102–112.

Jiang, J. S. & Brünger, A. T. (1994). *J. Mol. Biol.* **243**, 100–115.

Jones, T. A. (1982). *Computational Crystallography*, edited by D. Sayre, pp. 303–317. Oxford: Clarendon Press.

Jones, T. A., Zou, J. Y., Cowan, S. W. & Kjeldgaard, M. (1990). *Acta Cryst.* A**47**, 110–119.

Kirkman, H. N. & Gaetani, G. F. (1984). *Proc. Natl Acad. Sci. USA*, **81**, 4343–4347.

Ko, T.-P., Day, J., Malkin, A. J. & McPherson, A. (1999). *Acta Cryst.* D**55**, 1383–1394.

Kraulis, P. J. (1991) *J. Appl. Cryst.* **24**, 946–950.

Laskowski, R. A., MacArthur, M. W., Moss, D. S. & Thornton, J. M. (1993). *J. Appl. Cryst.* **26**, 283–291.

Luzzati, P. V. (1952). *Acta Cryst.* **5**, 802–810.

McPherson, A. (1982). *The Preparation and Analysis of Protein Crystals.* New York: John Wiley.

Malkin, A. J., Kuznetsov, Y. G., Land, T. A., DeYoreo, J. J. & McPherson, A. (1995). *Nature Struct. Biol.* **2**, 956–959.

Mann, H., McCoy, M. T., Subramaniam, J., Remmen, H. V. & Cadet, J. L. (1997). *Brain Res.* **770**, 163–168.

Maté, M. J., Lombardía, M. O., Marina, A. & Fita, I. (1999). *Acta Cryst.* D**55**, 1066–1069.

Maté, M. J., Zamocky, M., Nykyri, L. M., Herzog, C., Alzari, P. M., Betzel, C., Koller, F. & Fita, I. (1999). *J. Mol. Biol.* **286**, 135–149.

Matthews, B. W. (1968). *J. Mol. Biol.* **33**, 491–497.

Merritt, E. A. & Murphy, M. E. P. (1994). *Acta Cryst.* D**50**, 869–873.

Morikofer-Zwez, S., Gantz, M., Kaufman, H., von Wartburg, J. P. & Aebi, H. (1969). *Eur. J. Biochem.* **11**, 49–57.

Murthy, M. R. N., Reid, T. J., Sicignano, A., Tanaka, N. & Rossmann, M. G. (1981). *J. Mol. Biol.* **152**, 465–499.

Navaza, J. (1994). *Acta Cryst.* A**50**, 157–163.

Nicholls, A., Sharp, K. A. & Honig, B. (1991). *Proteins*, **11**, 281–296.

Quan, F., Korenluk, R. G., Tropak, M. B. & Gravel, R. A. (1986). *Nucleic Acids Res.* **14**, 5321–5335.

Quilliet, X., Chevallier-Lagente, O., Zeng, L., Calvayrac, R., Mezzzina, M., Sarasin, A. & Vuilaume, M. (1997). *Mutat. Res.* **385**, 235–242.

Sato, A., Furuno, T., Toyoshima, C. & Sasabe, H. (1993). *Biochem. Biophys. Acta*, **1162**, 54–60.

Scandalios, J. G. (1997). Editor. *Oxidative Stress and the Molecular Biology of Antioxidant Defenses.* Plainview, NY: Cold Spring Harbor Laboratory Press.

Sevinc, M. S., Maté, M. J., Switala, J., Fita, I. & Loewen, P. C. (1999). *Protein Sci.* **8**, 490–498.

Takeuchi, A., Miyamoto, T., Yamaji, K., Masuho, Y., Hayashi, M., Hayashi, H. & Onozaki, K. (1995). *Cancer Res.* **55**, 1586–1589.

Wilson, A. J. C. (1950). *Acta Cryst.* **3**, 397–398.